Pergamon

Cement and Concrete Research, Vol. 28, No. 10, pp. 1467–1477, 1998

0008-8846/98 $19.00 + .00

PII S0008-8846(98)00120-3

EFFECT OF SHRINKAGE AND MOISTURE CONTENT ON THE PHYSICAL CHARACTERISTICS OF BLENDED CEMENT MORTARS

V. Kanna,* R.A. Olson,* and H.M. Jennings[1]*†
*Department of Materials Science and Engineering, Northwestern University, Evanston, IL, USA
†Department of Civil Engineering, Northwestern University, Evanston, IL, USA

(Received August 7, 1997; in final form July 14, 1998)

ABSTRACT

The effects of drying on mortars containing Portland cement blended with fly ash or slag on the shrinkage, extent of surface cracking, pore size distribution as measured by mercury intrusion porosimetry, flexural strength, fracture toughness, and Young's modulus are reported. Specimens were exposed to conditions of 100% relative humidity (RH), 50% RH, and/or oven-drying at 105°C. Drying coarsened the pore structure and increased the density of surface cracks, but surprisingly increased the flexural strength and the fracture toughness, and as anticipated lowered the Young's modulus. This was regardless of the content of mineral admixture. © *1998 Elsevier Science Ltd*

Introduction

The strength and microstructure of concrete and mortar are known to be affected by drying, especially if they contain mineral admixtures such as fly ash or slag (1–6). The properties of blended cement products tend to improve slowly compared to ordinary Portland cement (OPC) products due to the relatively slow reaction rate of mineral admixtures. Also, if significant amounts of water are removed from a blended cement paste before it has matured, the inadequate curing conditions result in inferior properties and poor performance (1–6). Furthermore, the mechanical properties of a cement-based material at any age are generally a function of its moisture content. Drying has a great influence on the degree of shrinkage and the stress state of the system (7–9).

Drying shrinkage influences many different levels of the microstructure, but affects the mechanical properties in two basic ways. In one respect, it tends to increase strength by increasing surface energy and increasing bonding between particles of C-S-H (10,11). In another respect, since it is a quasi-brittle material, the strength should be reduced by microcrack formation. The extent of cracking depends upon the severity of drying, the rate of drying, and the sample geometry. Stress gradients develop within a cement-based material because drying first occurs at the surface and then proceeds inward. This causes tensile

[1]To whom correspondence should be addressed.

TABLE 1
Chemical compositions of cementitious components (in wt%).

Component	OPC	Slag	Fly Ash
SiO_2	22.2	38.1	43.9
CaO	64.5	39.0	5.3
MgO	1.1	10.6	1.5
Al_2O_3	3.2	8.2	24.9
Fe_2O_3	4.2	0.36	6.0
Na_2O	0.15	0.26	0.58
K_2O	0.52	0.35	0.83
S (total)	2.1	1.0	0.95

stresses to develop on the outside and compressive stresses on the inside; the larger the stress gradient, the greater the extent of cracking.

The goal of this paper is to report how certain properties of mortars containing slag or fly ash are affected by drying after the initial hardening process is complete. The mortars were cured for 7 days in saturated lime water before they were exposed to drying in order to insure that a significant degree of hydration occurred. Therefore, to a first approximation, different systems could be compared. A curing period of 7 days is considered to be critical for adequate hydration of blended cements containing fly ash or slag (5,6). Shrinkage was monitored continuously and the fracture toughness, flexural strength, pore size distribution, and extent of surface cracking were evaluated after drying. Because there are differences in the degree of reaction and other characteristics of the various samples in this research, the main results reported here are trends which appear worthy of analysis.

Experimental Procedures

Materials and Sample Preparation

Type I OPC and silica sand were the basic components of the mortars. Water absorption of the sand was found to be 0.025% according to ASTM C 128–88. The chemical compositions of the Class F fly ash and ground granulated blast furnace slag (hereafter referred to as slag) are given in Table 1. The densities of the cement, fly ash, and slag according to ASTM C 188–84 were found to be 3.07, 2.26, and 2.75 g/cm^3, respectively.

The pastes had a water-to-cementitious solids mass ratio (w/c) of 0.45, and the mortars had a sand-to-cementitious solids mass ratio of 1. OPC was replaced by 35 vol.% fly ash or slag in the blended cements. Mix parameters are given in Table 2. The total amount of water was adjusted to accommodate for absorption by the sand. All samples were cast as rectangular bars and compacted using a table vibrator. The samples used for shrinkage measurements had dimensions of 305 mm $\times$ 76 mm $\times$ 25 mm, and the samples used in the flexural and three-point bend tests had dimensions of 229 mm $\times$ 76 mm $\times$ 25 mm.

TABLE 2
Mix parameters of the mortars used in the three-point bend and flexural tests (in kg).

Batch	Cement	Sand	DI water	Fly ash	Slag
OPC	4.00	4.00	1.90	—	—
fly ash	2.60	3.63	1.72	1.03	—
slag	2.60	3.88	1.82	—	1.28

Specimen Conditioning

The samples were demolded 24 h after casting, submerged in lime-saturated water for 7 days at room temperature, and then subjected to one of the four conditions in Table 3. An oven-drying period of 6 days was sufficient time for specimens to reach a relatively constant weight. A water-cooled band saw was used to cut a 17 mm notch in each of the three-point bend test samples at 7 days before being subjected to drying.

Analytical Procedures

The relative moisture content was defined as the ratio of the water content of a sample to that of a fully saturated sample. The weight change after drying at 105°C for 24 h was used to calculate the evaporable water content of the conditioned mortars.

In the shrinkage samples, two stainless steel inserts were cast 254 mm apart. The change in length of these inserts was used to determine the strain. Two samples were used to obtain an average strain value for each condition.

Paste samples of the same w/c ratio as the mortars were subjected to the same conditions and analyzed using mercury intrusion porosimetry (MIP). Each conditioned sample was D-dried for 48 h before intrusion. Pressure ranged from ambient to 220 MPa.

Surface cracking was examined using a stereomicroscope at 40×. Cracks in a 127 mm × 25 mm area were traced with a permanent marker and photographed. The pictures were analyzed using a standard stereological procedure (12). The number of point intersections per unit length of test line (i.e. crack density) was determined for each sample.

Procedures described in ASTM C 293–79 were used to measure flexural strength. The

TABLE 3
Drying conditions (DC) for each sample set.

Condition	Procedure
control	Saturated lime water for 21 days (never dried)
DC1	50% RH for 21 days
DC2	Saturated lime water for 21 days followed by 6 days in an oven at 105°C
DC3	50% RH for 21 days followed by 6 days in an oven at 105°C

TABLE 4
Relative moisture content (%) for each mortar.

Batch	Control	DC1	DC2	DC3
OPC	100	72	4.7	3.9
fly ash	100	52	4.0	3.8
slag	100	67	8.5	5.9

experimentally derived Two Parameter Fracture Model (13–14) was used to determine the critical stress intensity factor (K_{Ic}) considering stable crack growth. A loading rate of 0.003 mm/min was used in the three-point bend tests.

Results and Discussion

Drying Shrinkage

Table 4 gives the relative moisture contents for the samples exposed to the drying conditions listed in Table 3. A wide range of moisture contents were measured at the time of testing. Figure 1 displays shrinkage as a function of time for the samples exposed to the drying conditions listed in Table 3. For each sample set a control sample was cured continuously at 100% RH. The amount of macroscopic shrinkage and the shrinkage rate varied between drying conditions. Samples exposed to conditions DC1 and DC2 (Table 3) produced about the same amount of shrinkage by 40 days in all the systems, but the rate of shrinkage was much greater with drying condition DC2. The slag system showed the greatest difference between conditions DC1 and DC2, with condition DC1 being about 0.3% less. Drying condition DC3, which had the greatest amount of shrinkage by 40 days, generated two stages of shrinkage; one during exposure to 50% RH between 7 and 28 days and another during drying at 105°C after 28 days.

Surface Cracking

Table 5 gives the crack density for each mortar. A small number of cracks were observed in the control samples. These may have developed during observation or could be a result of the small degree of expansion in these samples. The slag mortar control sample showed the greatest expansion and the greatest crack density of 15.8 cm^{-1}, while the fly ash mortar control sample showed the smallest expansion and the lowest crack density of 6.3 cm^{-1}.

All three systems displayed an increase in crack density as the drying conditions became more severe. Drying condition DC1 more than doubled the crack density in the OPC mortar as compared to the control, but increased the crack density almost 4 times in the slag mortars and almost 7 times in the fly ash mortars as compared to their control samples.

Although the amount of shrinkage for the samples exposed to drying conditions DC1 and DC2 were about the same, the rate of shrinkage for the samples exposed to condition DC2 was higher than that for condition DC1 and the crack density was greater, over 2 times for

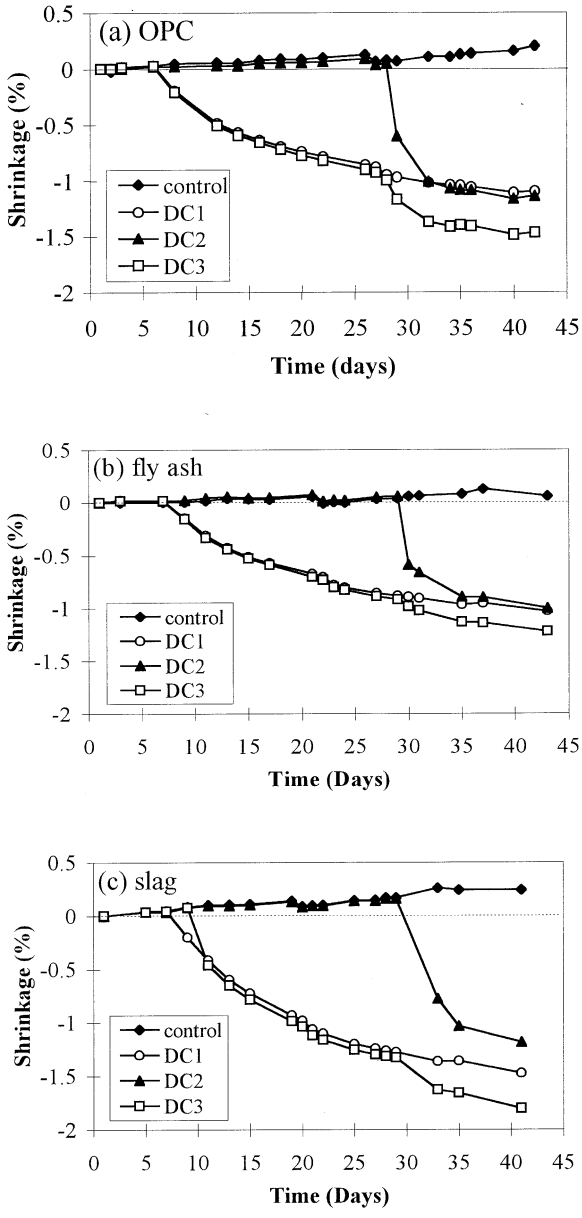

FIG. 1.
Shrinkage vs. time for the (*a*) OPC, (*b*) fly ash, and (*c*) slag mortars.

the blended cement mortars and over 4 times for the OPC mortar. Since the bulk shrinkage is about the same in these samples (between 1 and 1.5%), but the crack density varies greatly, it stands to reason that there is greater shrinkage on the microscopic level in the samples with a higher crack density, but the shrinkage is restrained so that the bulk shrinkage on the

TABLE 5
Crack density (cm^{-1}) for each mortar.

Condition	OPC	fly ash	slag
control	8.2	6.3	15.8
DC1	17.7	42.6	57.9
DC2	86.2	98.8	125.6
DC3	188.9	143.6	103.8

macroscopic level is controlled by the restraint in the microstructure even though part of the matrix shrinks extensively.

In drying condition DC3, the crack density for the OPC mortar was the greatest followed by the fly ash and the slag mortar, opposite to the trends in conditions DC1 and DC2. Apparently, the combination of drying at 50% RH and oven drying greatly increased the shrinkage on the microscopic level in the OPC mortars. The slag mortar displayed the greatest bulk shrinkage at 40 days (1.8%), but surprisingly it also displayed the lowest crack density. In comparing the crack density of the slag mortar in condition DC3 to conditions DC1 and DC2, it appears that slag mortar is more affected by drying rate than the level of drying, which is probably the reason for the low crack density.

Mercury Intrusion Porosimetry

The pore size distribution (PSD) curves for the OPC, fly ash, and slag cement pastes are shown in Figure 2. For the OPC mortars in Figure 2a, the sample exposed to condition DC1 is much coarser than the control sample (hydrated continuously at 100% RH) due to a combination of suppressed hydration from the lack of water at 50% RH (hydration is very slow below 80% RH) and the introduction of shrinkage cracks. Although the bulk shrinkage was about the same for all the samples exposed to conditions DC1 and DC2 and the degree of hydration was certainly greater for condition DC2, the shrinkage rate was greater for the sample exposed to condition DC2 and so was the crack density. Hence, the coarser PSD in this case must be a result of the presence of microcracks. The samples exposed to conditions DC2 and DC3 have identical PSDs, suggesting that the coarsening of the pore structure depends on oven-drying only.

In Figure 2b, the PSD of the control sample for the blended fly ash paste was very similar to the OPC control sample. The PSD of the blended fly ash sample exposed to drying condition DC1 is coarser than that exposed to condition DC2, which is opposite to the OPC pastes. This indicates that the inadequate curing at 50% RH was more significant in producing a coarse pore structure than was oven-drying. The blended fly ash sample exposed to condition DC3 produced the coarsest PSD.

In Figure 2c, the control sample for the blended slag paste had a finer PSD than the OPC control sample. The blended slag pastes exposed to drying conditions DC1 and DC2 produced similar PSD curves, even though the amount of macroscopic shrinkage was slightly greater for condition DC1. The blended slag paste exposed to condition DC3 had a much coarser PSD than any of the other samples tested, indicating that the combination of

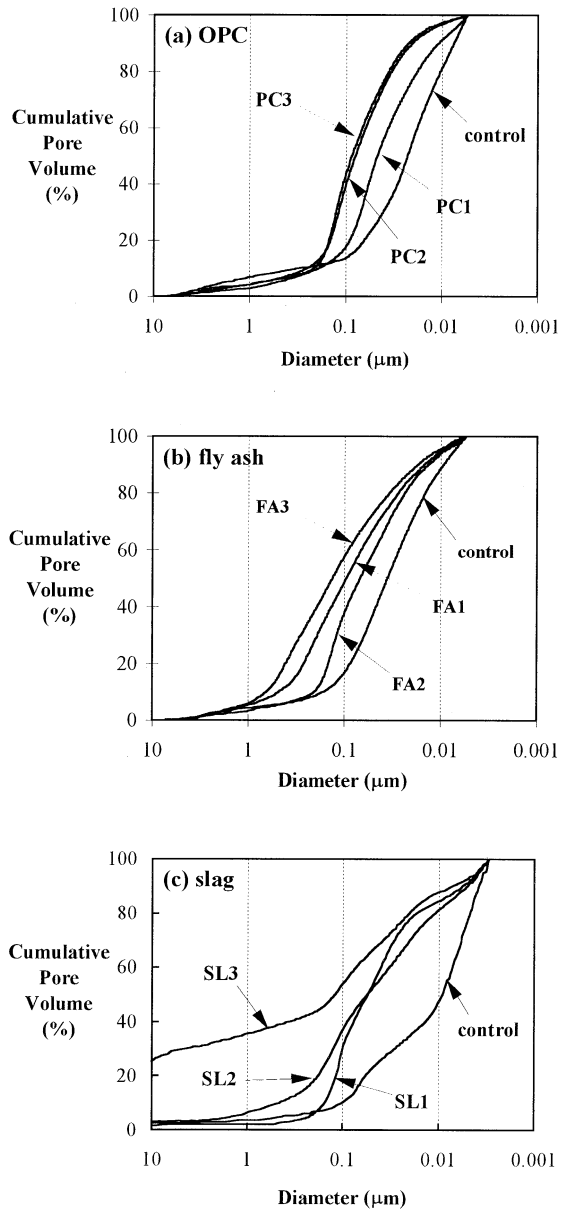

FIG. 2.
MIP curves for the (*a*) OPC, (*b*) fly ash, and (*c*) slag mortars.

inadequate curing at 50% RH and drying at 105°C had a drastic effect on the pore structure. This data combined with the relatively low crack density and high bulk shrinkage in the mortar exposed to the same conditions suggests that fewer but rather large cracks are forming in the blended slag paste. On the other hand, we also believe that MIP can sometimes be

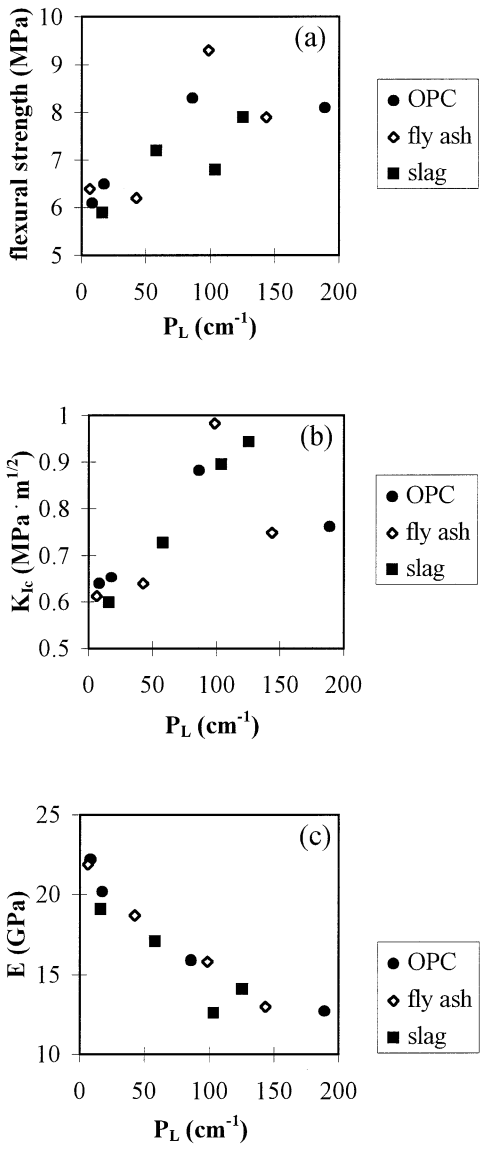

FIG. 3.
(*a*) Flexural strength, (*b*) K_{Ic}, and (*c*) Young's modulus as a function of crack density.

misleading (15,16) and that parts of the microstructure may have weakened to the point where they cannot withstand the high pressures inherent in the MIP procedure, which may apply to this case. In either case, drying condition DC3 inflicts a considerable amount of damage on the pore structure.

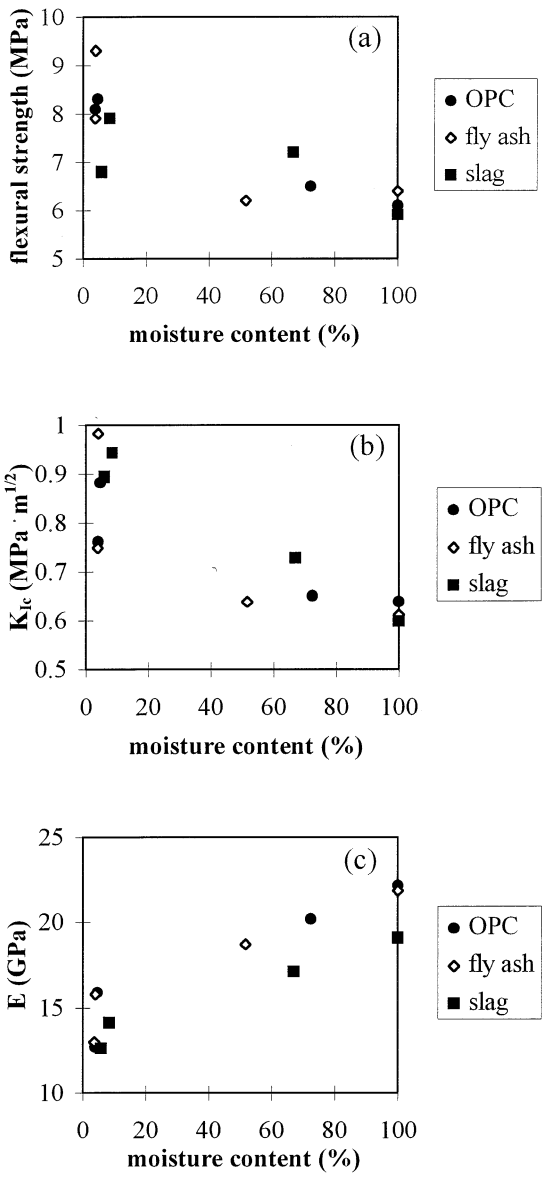

FIG. 4.
(*a*) Flexural strength, (*b*) K_{Ic}, and (*c*) Young's modulus vs. moisture content.

Mechanical Properties

Cracking should have a detrimental effect on the mechanical properties, but a trend contradictory to expectations is observed. As shown in Figures 3a and 3b, the flexural strength and toughness increased as the crack density increased. Since these materials are basically brittle

and therefore sensitive to flaws, this result is surprising. Therefore, these trends must be related to an increase in surface energy and interparticle bonding with drying (10,11).

Figure 4 shows the flexural strength, critical stress intensity factor, and Young's modulus for the three mortar systems as a function of relative moisture content. In Figure 4a, the flexural strength increased as the moisture content decreased, and although there is a slight variation, all three systems display similar flexural strengths regardless of mineral admixture. These results are in agreement with those of Mills (17), who showed that concrete strength decreased with moisture content, with those reported by Gopalan et al. (1) and Butler et al. (2), who did not find a significant difference between the 28 day flexural strength of OPC concrete and that containing fly ash, and with those of Haque et al. (18) and Fernandez et al. (19), who found similar flexural strengths in slag cement and OPC mortars between 7 and 91 days. The data presented here broadens the validity of these conclusions over a wider range of moisture contents and shows several properties of the same material.

The fracture toughness in Figure 4b followed a trend similar to the flexural strength behavior in that it increased with decreasing relative moisture content. In Figure 3b, the fracture toughness appears to reach a maximum at a crack density of about 100 cm^{-1} and then decrease. Hence, the toughening effect of increased surface energy and interparticle bonding with drying must be over-ridden at some point by crack formation at high crack density, indicating that extensive cracking is detrimental. In other words, some cracking may increase the size of a fracture zone and roughen the crack path, which would increase toughness, but eventually the crack density increases to the point where it controls toughness. From Griffith theory, the theoretical fracture strength (σ_f) is expressed as:

$$\sigma_f = \left(\frac{\gamma E}{\pi(2C)}\right)^{1/2} \propto \left(\frac{K_{Ic}}{C}\right)^{1/2}$$

where E = Young's Modulus, γ = surface energy, and $2C$ = critical crack length. Since C increases and E decreases upon drying, the surface energy must increase greatly upon drying. Both an increased process zone and an increase in the roughness of crack paths can achieve this.

The Young's modulus decreased with increasing crack density and decreasing moisture content throughout the entire range, as shown in Figures 3c and 4c. The Young's modulus of the slag mortar was slightly below that of the fly ash and OPC mortars. Although the flexural strength behavior was dominated by moisture content, the behavior of the Young's modulus was dominated by the formation of cracks; the greater the crack density, the less stiff the mortar.

Conclusions

The effect of drying on the characteristics of mortars containing fly ash or slag was studied. The flexural strength and fracture toughness increased even though crack formation increased with the severity of drying, indicating that interparticle bonding and effective surface energy, as related to roughness of crack path and size of the process zone, dominated the mechanical properties regardless of the presence or type of mineral admixture. Although there was considerable difference in shrinkage at the microscopic level between systems, as seen from the generally higher crack densities and the coarser pore size distributions upon drying in the

systems containing fly ash or slag, there was not much of a difference in the macroscopic shrinkage or the mechanical properties.

Acknowledgments

Financial support by the U.S. Department of Energy (grant number #DE-FG02–91ER45460/A01) is gratefully acknowledged.

References

1. M.K. Gopalan and M.N. Haque, ACI Mater. J. 84, 14, 14 (1987).
2. W.B. Butler and J.B. Ashby, ACI-RILEM Symposium, Universidad Autonoma de Neuvo Leon, 197, 1985.
3. M.N. Haque and O.A. Kayyali, ACI Mater. J. 86, 2, 128 (1989).
4. J.S. Sawan, J. Mater. Civ. Eng. 4, 2, 153 (1992).
5. M.N. Haque, Concr. Int. 12, 2, 42 (1990).
6. M.N. Haque and T. Chulilung, Cem. Concr. Res. 20, 120 (1990).
7. Y. Xi and H.M. Jennings, Materials Science of Concrete III, J.P. Skalny (ed.), Am. Ceram. Soc., Westerville, OH, p. 37, 1992.
8. H. Roper, Hwy. Res. Bd. Spec. Rpt. 90, 74 (1966).
9. W. Hansen, J. Am. Ceram. Soc. 70, 323 (1987).
10. C.D. Johnston and E.H. Sidwell, ACI Mater. J. 66, 748 (1969).
11. W.S. Butcher, Constructional Review (Sydney), 31, 12, 31 (1958).
12. Metals Handbook, H.E. Boyer and T.L. Gall (eds.), ASM, Metals Park, OH, 1985.
13. RILEM, "Determination of Fracture Parameters (K^S_{Ic} and CTODc) of Plain Concrete Using Three-Point Bend Tests," Materiaux et Constructions 23, 457, 1990.
14. Y. Jenq and S.P. Shah, J. Eng. Mech. 111, 1227 (1985).
15. R.F. Feldman, J. Am. Ceram. Soc. 67, 30 (1984).
16. R.A. Olson, C.M. Neubauer, and H.M. Jennings, J. Am. Ceram. Soc. 80, 2454 (1997).
17. R.H. Mills, International Symposium on Concrete and Reinforced Concrete in Hot Countries, Haifa, 1960.
18. F.J. Haque and J.W. Meusel, Cem. Concr. Aggr. 3, 40 (1981).
19. L. Fernandez and V.M. Malhotra, Cem. Concr. Aggr. 12, 2, 87 (1990).